Electrostatic Interference of Ruptured Coaxial Cable with Multiple Dielectrics

Jaeyul Choo*, Hyun Shin Park, and Youngsik Cho
Korea Institute of Nuclear Safety, 62 Gwahak-ro, Yuseong-gu, Daejeon, Korea
**Corresponding author: k728cjy@kins.re.kr*

1. Introduction

A coaxial cable is generally used as a transmission line for a signal of communication in a radio frequency band. The coaxial cable is composed of a central metallic-core, an intermediate dielectric-insulator surrounded a metallic-shield, and an outer dielectric-jacket as shown in Fig. 1. The coaxial cable transmits the signal using the electromagnetic field confined to the dielectric-insulator between the central metallic-core and the metallic-shield. In addition, the coaxial cable provides several advantages such as the good protection from electromagnetic interference by the metallic-shield.

Thanks to such good characteristics, the coaxial cables have been employed well in industrial facilities including a nuclear power plant. However the coaxial cable simultaneously poses an on-going challenge because the deterioration in shielding performance caused by environmental damages (thermal and pressure shock, etc.) results in the undesired electromagnetic interference and susceptibility (EMI/EMS) problems between a coaxial cable and adjacent equipment. In [1] the startup-range neutron monitoring (SRNM) system is suffered from the electromagnetic noise coupled with the control cable for a fine-motion control rod drive (FMCRD) in a nuclear reactor. To alleviate the EMI problem, a robust shield and a low pass filter are employed instead of increasing the separation-distance between the coupled cables in [1].

As another study for shielding performance, we perform the electromagnetic analysis for the coaxial cable using the mode-matching method. In our analysis, we assume that the coaxial cable has multiple inner and outer dielectrics and is ruptured along the length of the coaxial cable [2]-[4]. Based on the Laplace's equation and the superposition principle in the mode-matching method, we formulates potential and then enforces the Dirichlet and Neumann boundary conditions. We then investigate the electric field distributions and the variation in the capacitance while the size of a slot on a metallic-shield changes. The computed results enable us to estimate how much the rupture coaxial cable is electromagnetically coupled with the nearby objects each other.

2. Mode-matching method

2.1 Explanation of Slotted Coaxial Cable

Fig. 2 illustrates the cross section of the ruptured coaxial cable that is composed of a central metallic-core at a potential V_1, inner-dielectric layers of (n + 1) for insulator as regions *is* and *i*1–*in*, a single metallic layer

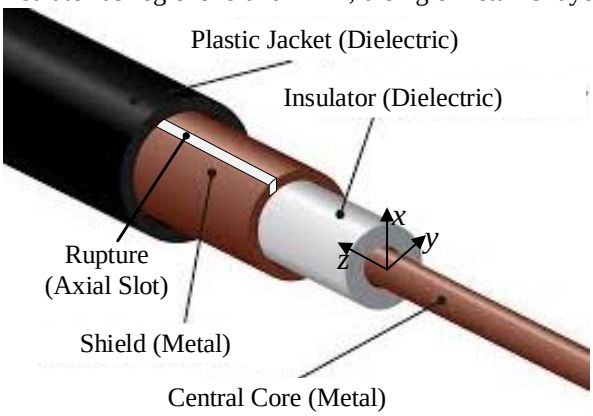

Fig. 1. Configuration of the ruptured coaxial cable.

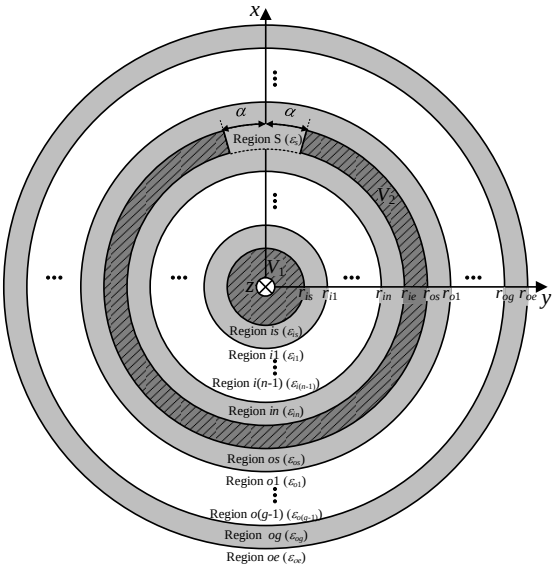

Fig. 2. Cross section of the ruptured coaxial cable.

for a shield at a potential V_2, and outer-dielectric layers of (g + 1) for a jacket as regions *os* and *o*1–*og*. We assume that the coaxial cable, which is infinitely extended in the *z*-direction, is ruptured in the form of an axial slot with the slot angle 2α as region *s* and surrounded by a free space as region *oe*. To be specific, the dielectric constant and radius for each region are defined as ε_R and r_R (R = *is*, *i*1, …, *in*, *s*, *os*, *o*1, …*og*, *oe*) in Fig. 2.

2.2 Expression of Potential

The potential for each region in Fig. 2 is governed by the Laplace's equation in cylindrical coordinates as

$$\nabla^2\Phi = \left(\frac{\partial^2}{\partial\rho^2} + \frac{1}{\rho}\frac{\partial}{\partial\rho} + \frac{1}{\rho^2}\frac{\partial^2}{\partial\phi^2}\right)\Phi(\rho)\Phi(\phi) = 0 \quad (1)$$

We utilize separation variables in conjunction with superposition principle for three cases where there exist only V_1 (V_2 = 0), only V_2 (V_1 = 0), and both V_1 and V_2, respectively [2]. The derived potentials in regions *is*, *s*, *os*, *oe* are expressed as, respectively,

$$\Phi_{is} = A_{is,0}\ln\left(\frac{\rho}{r_{is}}\right) + V_1 + \sum_{m_{is}=1}^{m_{is}=M_{is}} A_{is,m_{is}}\left(\left(\frac{\rho}{r_{is}}\right)^{-m_{is}} - \left(\frac{\rho}{r_{is}}\right)^{m_{is}}\right)\cos m_{is}\phi \quad (2)$$

$$\Phi_s = \sum_{m_s=1}^{m_s=M_s}(A_{s,m_s}\rho^{-\nu} + B_{s,m_s}\rho^{\nu})\sin\nu(\phi+\alpha) + V_2 \quad (3)$$

$$\Phi_{os} = A_{os,0} + B_{os,0}\ln\rho + \sum_{m_{os}=1}^{m_{os}=M_{os}}(A_{os,m_{os}}\rho^{-m_{os}} + B_{os,m_{os}}\rho^{m_{os}})\cos m_{os}\phi \quad (4)$$

$$\Phi_{oe} = A_{oe,0} + \sum_{m_{oe}=1}^{m_{oe}=M_{oe}} A_{oe,m_{oe}}\rho^{-m_{oe}}\cos m_{oe}\phi \quad (5)$$

where M_{is}, M_s, M_{os}, and M_{oe} are the number of the maximum mode in each region and $\nu = m_s / 2\alpha$

In addition, the potentials in regions *i*1–*in* and *o*1–*og* for multiple dielectrics are expressed as, respectively,

$$\Phi_{iq} = A_{iq,0} + B_{iq,0}\ln\rho + \sum_{m_{iq}=1}^{m_{iq}=M_{iq}}(A_{iq,m_{iq}}\rho^{-m_{iq}} + B_{iq,m_{iq}}\rho^{m_{iq}})\cos m_{iq}\phi \quad (6)$$

$$\Phi_{ok} = A_{ok,0} + B_{ok,0}\ln\rho + \sum_{m_{ok}=1}^{m_{ok}=M_{ok}}(A_{ok,m_{ok}}\rho^{-m_{ok}} + B_{ok,m_{ok}}\rho^{m_{ok}})\cos m_{ok}\phi \quad (7)$$

where M_{iq} and M_{ok} are the number of the maximum mode in regions *q* and *k* (*q* = 1, 2, …, *n* and *k* = 1, 2, … *g*).

2.3 Enforcement of Boundary Condition

The unknown modal coefficients of A_{is}, A_{iq}, B_{iq}, A_s, B_s, A_{os}, B_{os}, A_{ok}, B_{ok}, and A_{oe} in (2)–(7) can be determined by enforcing Dirichlet and Neumann boundary conditions on the continuities of the potential and the normal derivative of potential at $r = r_{iq}$ (*q* = 1, …, *n*), $r = r_{ie}$, $r = r_{os}$, and $r = r_{ok}$ (*k* = 1, …, *g*), $r = r_{oe}$.

The Dirichlet and Neumann boundary conditions at $r = r_{iq}$ (*q* = 1, …, *n*) between the inner regions *is* and *iq* are represented as

$$\Phi_{is}\big|_{\rho=r_{i1}} = \Phi_{i1}\big|_{\rho=r_{i1}}, -\alpha \le \phi < 2\pi - \alpha \quad (8)$$

$$\Phi_{i(b-1)}\big|_{\rho=r_{ib}} = \Phi_{ib}\big|_{\rho=r_{ib}}, -\alpha \le \phi < 2\pi - \alpha \quad (9)$$

$$\varepsilon_{is}\frac{d\Phi_{is}}{d\rho}\bigg|_{\rho=r_{i1}} = \varepsilon_{i1}\frac{d\Phi_{i1}}{d\rho}\bigg|_{\rho=r_{i1}}, -\alpha \le \phi < 2\pi - \alpha \quad (10)$$

$$\varepsilon_{i(b-1)}\frac{d\Phi_{i(b-1)}}{d\rho}\bigg|_{\rho=r_{ib}} = \varepsilon_{ib}\frac{d\Phi_{ib}}{d\rho}\bigg|_{\rho=r_{ib}}, -\alpha \le \phi < 2\pi - \alpha \quad (11)$$

where *b* = 2, 3, …, *n*.

The Dirichlet and Neumann boundary conditions at $r = r_{ie}$ between the regions *in* and *s* are represented as

$$\Phi_{in}\big|_{\rho=r_{ie}} = \begin{cases} V_2 & , \quad \alpha < \phi < 2\pi - \alpha \\ \Phi_s\big|_{\rho=r_{ie}} & , \quad -\alpha < \phi < \alpha \end{cases} \quad (12)$$

$$\varepsilon_{in}\frac{d\Phi_{in}}{d\rho}\bigg|_{\rho=r_{ie}} = \varepsilon_s\frac{d\Phi_s}{d\rho}\bigg|_{\rho=r_{ie}}, -\alpha < \phi < \alpha \quad (13)$$

The Dirichlet and Neumann boundary conditions at $r = r_{os}$ and $r = r_{ok}$ (*k* = 1, …, *g*) are analogous to (8) – (13). In case of the boundary at $r = r_{oe}$, the Dirichlet and Neumann boundary conditions are obtained as

$$\Phi_{og}\big|_{\rho=r_{oe}} = \Phi_{oe}\big|_{\rho=r_{oe}}, -\alpha \le \phi < 2\pi - \alpha \quad (14)$$

$$\varepsilon_{og}\frac{d\Phi_{og}}{d\rho}\bigg|_{\rho=r_{oe}} = \varepsilon_{oe}\frac{d\Phi_{oe}}{d\rho}\bigg|_{\rho=r_{oe}}, -\alpha \le \phi < 2\pi - \alpha \quad (15)$$

The results from the enforcement of boundary conditions constitute a set of simultaneous equations to determine the model coefficients A_{is}, A_{iq}, B_{iq}, A_s, B_s, A_{os}, B_{os}, A_{ok}, B_{ok}, and A_{oe}. After checking the convergence of the potentials in each region using the determined modal coefficients, we truncated the maximum mode numbers M_{is}, M_s, M_{os}, M_{oe}, M_{iq}, and M_{ok} to achieve efficient computation.

3. Computed results

Various electromagnetic characteristics such as electric field and capacitance were spontaneously calculated by the obtained modal coefficients. Electrical field is derived from the calculated potential as

$$\overline{E} = -\nabla\Phi = \hat{a}_\rho E_\rho + \hat{a}_\phi E_\phi = \hat{a}_\rho\left(-\frac{\partial\Phi}{\partial\rho}\right) + \hat{a}_\phi\left(-\frac{1}{\rho}\frac{\partial\Phi}{\partial\phi}\right) \quad (16)$$

In addition, the total charge and capacitance per unit length are calculated by

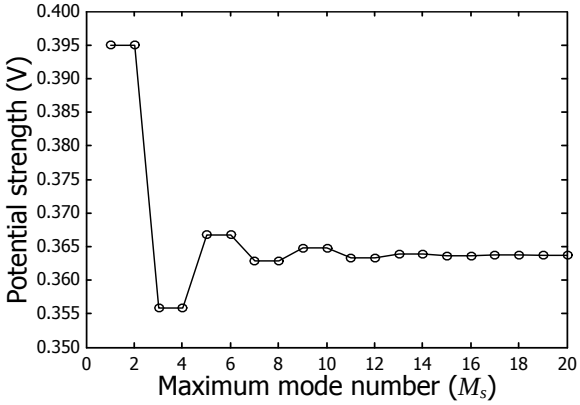

Fig. 3. Convergence of potential Φ_s at $\rho = 22$ mm and $\phi = 0°$.

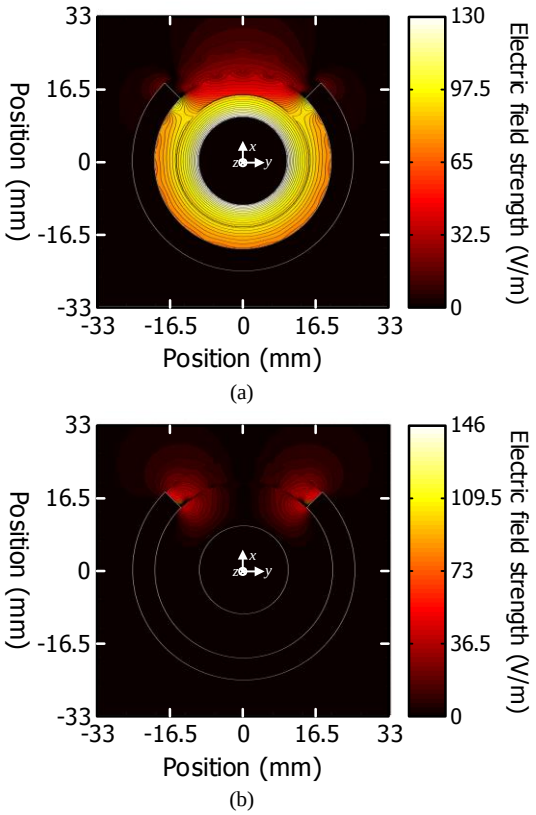

Fig. 4. Computed electrical field strength (a) Electric field strength of E_ρ. (b) Electric field strength of E_ϕ.

$$Q = \varepsilon_1 \int_{-\alpha}^{2\pi-\alpha} \left[-\nabla\Phi_1(\theta,\phi)\right] \cdot \hat{\rho}\rho d\phi = -2\pi\varepsilon_1 A_{10} \tag{17}$$

$$C = \frac{-2\pi\varepsilon_1 A_{10}}{V_1 - V_2} \tag{18}$$

We investigated the distributions of the electric fields and the capacitances of the ruptured coaxial cable with two layers of the inner dielectrics and a single layer of the outer dielectric (n = 1 and k = 1). The design parameters of the computed coaxial cable with a slot are $M_{is} = M_{i1} = M_s = M_{os} = M_{o1} = M_{oe} = 20$, $V_1 = 1$ V, $V_2 = 0$ V, $r_{is} = 10$ mm, $r_{i1} = 15$ mm, $r_{ie} = 20$ mm, $r_{os} = 25$ mm,

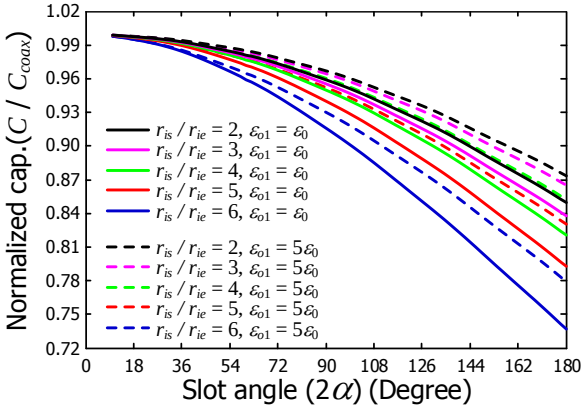

Fig. 5. Cross section of the ruptured coaxial cable.

$r_{o1} = 42.5$ mm, $r_{oe} = 47.5$ mm $\alpha = 22.5°$, and $\varepsilon_{is} = \varepsilon_{i1} = \varepsilon_s = \varepsilon_{os} = \varepsilon_{o1} = \varepsilon_{oe} \approx 8.854 \times 10^{-12}$.

We examined the convergence of the infinite series solution for the potential at $\rho = 22$ mm and $\phi = 0°$ in Fig. 3 while the maximum mode number M_s increases up to 20. In Fig. 3, we confirmed that the potential strength converges on 0.364 V while the maximum mode number M_s approaches to 20. This fast convergence is enable to analyze the slotted coaxial cable by truncating the maximum mode numbers efficiently.

We computed the electrical field distributions of the slotted coaxial cable with the same design parameters in Fig. 3. The computed electric field distributions in terms of E_ρ and E_ϕ are shown in Figs. 4(a) and 4(b), respectively. As expected, the electrical field is formed outside of the coaxial cable through the axial slot. The leaky electrical field possibly causes an electromagnetic interference (EMI) problem to adjacent objects. In comparison between Figs. 4(a) and 4(b), while E_ρ is stronger than E_ϕ inside of the coaxial cable, E_ϕ changes to be dominant near the edge of the slot.

In addition, we calculated the capacitances of slotted coaxial cable for different dielectrics in region $o1$ (cases of $\varepsilon_{o1} = \varepsilon_0$ and $\varepsilon_{o1} = 5\varepsilon_0$) when the slot angle 2α increases from 10° to 180° and the ratio of r_{is} / r_{ie} steps up from 2 to 6 in the same design condition of Fig. 3. The investigated capacitances per unit length are represented in Fig. 5 where the capacitances are normalized by the capacitance ($C_{coax} = 2\pi\varepsilon_{is} / \ln(r_{ie} / r_{is})$) of the normal coaxial cable without the slot. It is seen that the normalized capacitance decreases as either the ratio of r_{is} / r_{ie} increases or dielectric constant ε_{o1} decreases. As expected, the normalized capacitance increases while the slot angle 2α varies from 180° to 0°, and then approaches 1 which implies that the capacitance of the slotted coaxial cable nearly equals to that of the normal coaxial cable. Note that additional computations in variation of other design parameters

provide us with the useful information to alleviate EMI problems.

4. Conclusions

We applied the mode-matching method to the quasi-static analysis of a slotted coaxial cable. After determining the maximum mode number based on the convergence of an infinite series solution, we investigated the distributions of electric field and the normalized capacitance in variation of a slot angle (2α) and a dielectric constant (ε_{o1}) in the outer dielectric region to obtain the useful information to build precaution against EMI problems

5. Acknowledgement

This work was supported by the Korea Institute of Nuclear Safety under the project “Development of Proof Test Model and Safety Evaluation Techniques for the Regulation of Digital I&C Systems used in NPPs” (no. 1305003−0315−SB130)

REFERENCES

[1] T. P. Wang and Z. W. Li, Significant Reduction of Electromagnetic Interference for Fine-motion Control Rod Drive in a Nuclear Reactor, IEEE Trans. Ind. Electron., Vol. 61, No. 10, pp. 5582-5589, Oct. 2014.
[2] D. Kim and H. J. Eom, Capacitance of Axially Slotted Coaxial Cable, Microwave and Optical Tech. Lett., Vol. 48, No. 4, pp. 825-827, Apr. 2006.
[3] S. H. Gurbaxani, V. E. Marthnez, and S. H. Nabavi, On the Solution of Periodic Cylindrical Structures with Mixed Boundary conditions, IEEE Trans. Electomag. Compat. Vol. 36, No. 1, pp. 74-76, Feb. 1994.
[4] H. J. Eom, Electromagnetic Wave for Boundary-Value Problem, Berlin, Germany: Springer Verlag, 2004.